frontiers in Materials

ORIGINAL RESEARCH
published: 14 March 2022
doi: 10.3389/fmats.2022.827476

Comparative Study on the Effect of Ultrasonic Power on the Microstructure and Mechanical Properties of 2195 Aluminum Alloy Ingot

Yuqi Hu[1,2], *Ripeng Jiang*[1,2]* *and Xiaoqian Li*[1,2]

[1]Research Institute of Light Alloy, Central South University, Changsha, China, [2]State Key Laboratory of High-Performance Complex Manufacturing, Central South University, Changsha, China

High-intensity ultrasound was introduced for the casting of 2195 aluminum–lithium alloy ingots. The shape of the ingots was a cylinder with a length of 650 mm and a radius of 30 mm. In this study, the effects of different ultrasonic powers were applied in the melt. The grain shape, α-Al grain size, the size of the precipitated phase, and the mechanical properties of the ingots were compared. The results showed that when the power of the ultrasonic system was maintained at 1,600 W, an ingot with a more uniformly dispersed precipitation phase and grain refinement structure was formed. It can be concluded that the coarse eutectic structure in the ingot is effectively reduced when the power is around 1,600 W, and the mechanical properties of the ingot reach the best value.

Keywords: high-intensity ultrasound, 2195 aluminum–lithium alloy, ultrasonic power, the mechanical properties, precipitation phase

OPEN ACCESS

Edited by:
Peng Cao,
the University of Auckland,
New Zealand

Reviewed by:
Liyuan Sheng,
Peking University, China
Jiangshan Zhang,
University of Science and Technology Beijing, China

***Correspondence:**
Ripeng Jiang
jiangrp@csu.edu.cn

Specialty section:
This article was submitted to Structural Materials, a section of the journal Frontiers in Materials

Received: *02 December 2021*
Accepted: *17 January 2022*
Published: *14 March 2022*

Citation:
Hu Y, Jiang R and Li X (2022) Comparative Study on the Effect of Ultrasonic Power on the Microstructure and Mechanical Properties of 2195 Aluminum Alloy Ingot. Front. Mater. 9:827476. doi: 10.3389/fmats.2022.827476

INTRODUCTION

By the 1990s, due to the increased demand for low cost, high efficiency, and lightweight alloys, many researchers have paid more attention to the study of aluminum–lithium alloy (Al–Li) materials (Blankenship and Kaisand, 1996). The 2195 Al–Li alloy has excellent performance and strength. It was used in the United States to replace the 2219 alloy in the storage tank of the space shuttle, which increased its aerospace carrying capacity to 3.4t (Jata et al., 1996). The ingot was processed into qualified aerospace parts. The ingot was first prepared into a suitable shape, and the corresponding parts could be obtained after forging and rolling processes. The basis of these studies was that excellent performance ingots were required. As a result, the casting process was one of the most important processes, which could influence the final structure and performance of the 2195 Al–Li alloy ingot. Recently, to improve the quality of ingots, researchers have applied many related technologies in the casting process, including physical methods (such as mechanical stirring and electromagnetic stirring) and chemical methods (such as adding nucleating agents). Among these methods, Eskin and Eskin (2014) and Abramov (1999) believed that ultrasonic treatment had higher efficiency and better effects in refining the solidification structure and changing the mechanical properties in the aluminum alloy melting process, so there was great potential for this engineering application.

Investigating the impact of high-intensity ultrasonic treatment on the structure, erosion, and mechanical behavior of the AC7A aluminum combination, El-Aziz et al. (2016) showed that the

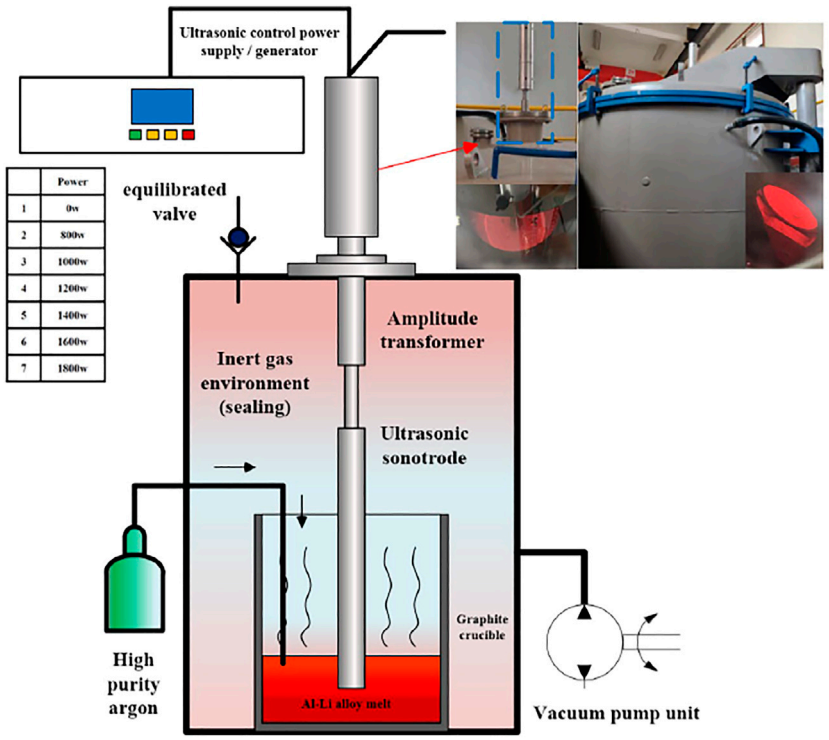

FIGURE 1 | Schematic diagram of the ultrasonic system.

solidification process under the activity of ultrasound could give fine round particles and metal compounds. Huang et al. (2014) showed that ultrasound has the effect of inhibiting nucleation and refining the grain structure and the structure refining effect decreases with the increase of the ultrasonic distance. Li et al. (2021) showed that simulation of the casting ultrasonic vibration system is carried out. It is found that the range and intensity of cavitation are inversely proportional to the distance of the radiation end face; at the same time, smaller cavitation domains will be discontinuously distributed in the radiation direction. In the process of preparing 2xxx series and 7xxx series large-diameter aluminum alloy ingots, the ultrasonic vibration system is effectively arranged, and the influence of ultrasonic system control, ultrasonic depth, and other parameters on the quality of large-diameter ingots is studied, and the leading ultrasonic preparation process parameters are proposed to achieve ultrasonic industrialization of casting.

Due to the active chemical characteristics of the Li element, Al–Li alloy ingots are prone to be lost during smelting and casting (Eswara Prasad et al., 2014). As a result, the traditional melt treatment method became more complex, and the ultrasonic melt treatment technique was introduced into the Al–Li alloy ingot casting process. However, most past studies have concentrated on using an ultrasonic technique to cast typical aluminum alloys. Al–Li alloy ingots, particularly 2195 Al–Li alloy ingots, have received little attention. This work investigated the influence of high-intensity ultrasonic radiation on the microstructure and mechanical characteristics of Al–Li alloy ingots. To determine the optimum ultrasonic power parameters, the 7-set ultrasonic power was employed in the casting process of 2195 Al–Li alloy ingots. The microstructure of α-Al grains and eutectic structures in ingots of various powers were compared using optical microscopes and SEM analytical techniques. In addition, the mechanical properties of the seven ingots were also examined and compared.

EXPERIMENTAL

As shown in **Figure 1**, it included the configuration of the ultrasonic system, the ultrasonic power setting, the deployment of ultrasonic probes, a typical industrial-grade vacuum casting platform, and an ultrasonic casting platform. The ultrasonic system incorporated an ultrasonic generator with a maximum output power of 2 kW, a 20 kHz piezoelectric transducer with an air cooler, an ultrasonic converter, and an ultrasonic vibrator composed of a titanium sonotrode with a diameter of 50 mm. The maximum vibration amplitude measured on the face of the ultrasonic generator was 20 μm. The chemical composition of the ultrasonic probe can be obtained from the reference (Rioja et al., 2012). Although there was only one sounder, the high-frequency vibration area was enough to affect all the melts in the crucible. Before adding the ultrasonic sonotrode to the aluminum melt, it was preheated at 300°C for 20 min, to make the output power supply quickly reach a stable state.

Before the ingot was prepared, the air in the melting furnace cavity was extracted, a vacuum pump unit was used, and the air pressure in the furnace cavity was measured with a resistance vacuum gauge to be

TABLE 1 | Contents of major elements in the as-received AA2195 Al alloy (wt%).

Elements	Al	Cu	Li	Mg	Ag	Zr	Mn	Fe	Si
Content	Bal	4.0	1.0	0.4	0.4	0.1	0.25	0.1	0.06

10 Pa (standard atmospheric pressure = 10.1×10^4 Pa). Then, the argon gas was introduced into the cavity at the standard atmospheric pressure. This solution allowed for a better reduction of the oxygen content in the furnace chamber. The raw materials used to prepare alloys in advance, such as Al–Cu alloy, Al–Zn alloy, high-purity aluminum, high-purity magnesium, high-purity silver, and high-purity lithium, were softened in a underneath resistance heater with argon environment, followed with mechanical stirring and expulsion of slag. At that point, the ultrasonic-aided casting framework was connected to the treated aluminum melt. In a previous research work by Li et al. (2014), the ultrasonic probe used was immersed 20 mm below the surface of the melt during the casting process. After 30 min of ultrasonic treatment, the aluminum melt was introduced into the mold for casting. The 2195 Al–Li alloy ingot was successfully manufactured, and its nominal composition is shown in **Table 1**.

CHARACTERIZATION

After the natural aging treatment, a circular plate with a thickness of 20 mm was cut transversely from two parts of the seven ingots. As shown in **Figure 2**, a sample for microstructure analysis was obtained at a specific position in the axial and radial directions. To test the mechanical properties, samples were taken at the radial and axial positions of the ingot at the same time.

Determination of Mechanical Properties

From the top and bottom of the 2195 Al–Li alloy ingot, a dog bone-shaped tensile sample was processed. To explore the anisotropy of the material, samples were taken in the axial and radial directions, respectively. As shown in **Figure 2**, to reduce the influence of surface roughness on tensile properties, the diamond suspension was used to perform good mechanical polishing on all tensile samples. The standard size of the dog bone tensile sample is shown in **Figure 2**. The tensile test was carried out in the Instron test 3369 machine at a displacement rate of 2.0 mm/min at room temperature. In addition, the extensometer was used to measure the strain of the tensile sample.

Microstructural Characterization at Multiscale

A metallographic sample was taken from the as-cast AA2195 ingot. The samples were mechanically ground, polished, and etched according to the method proposed by Zhang et al. (2019). The microstructure was characterized by a scanning electron microscope (SEM; TESCAN, MIRA3 MMH/MMU) equipped with an energy dispersive spectroscopy (EDS). Metallographic phase observation was performed in polarization light with a ZEISS optical microscope equipped with an automatic Zeiss AxioVision image analyzer. The grain measure was based on

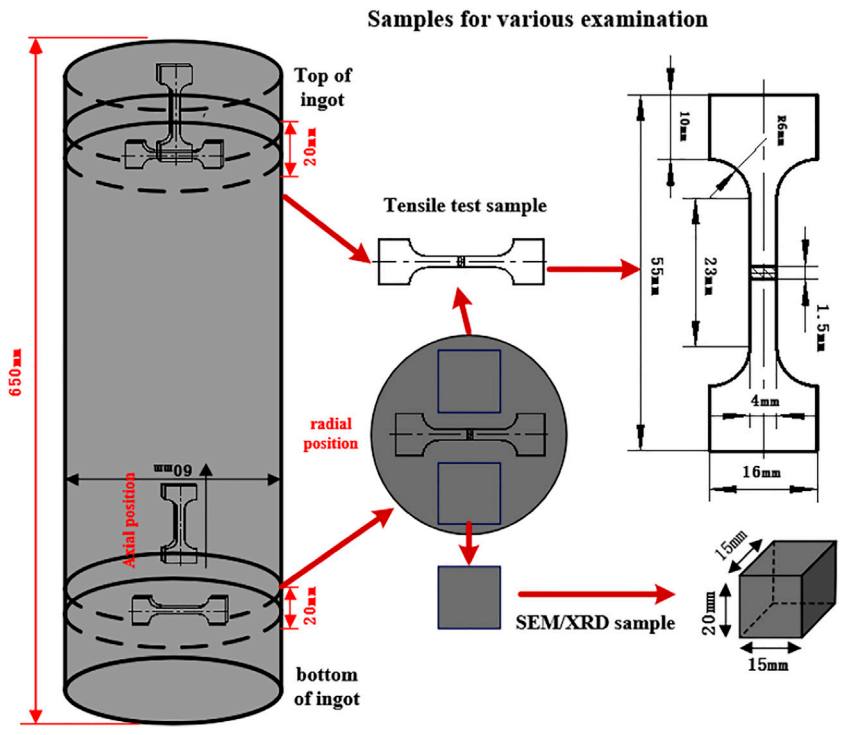

FIGURE 2 | Schematic graph showing agent positions of microstructure tests and ductile tests taken from the ingot.

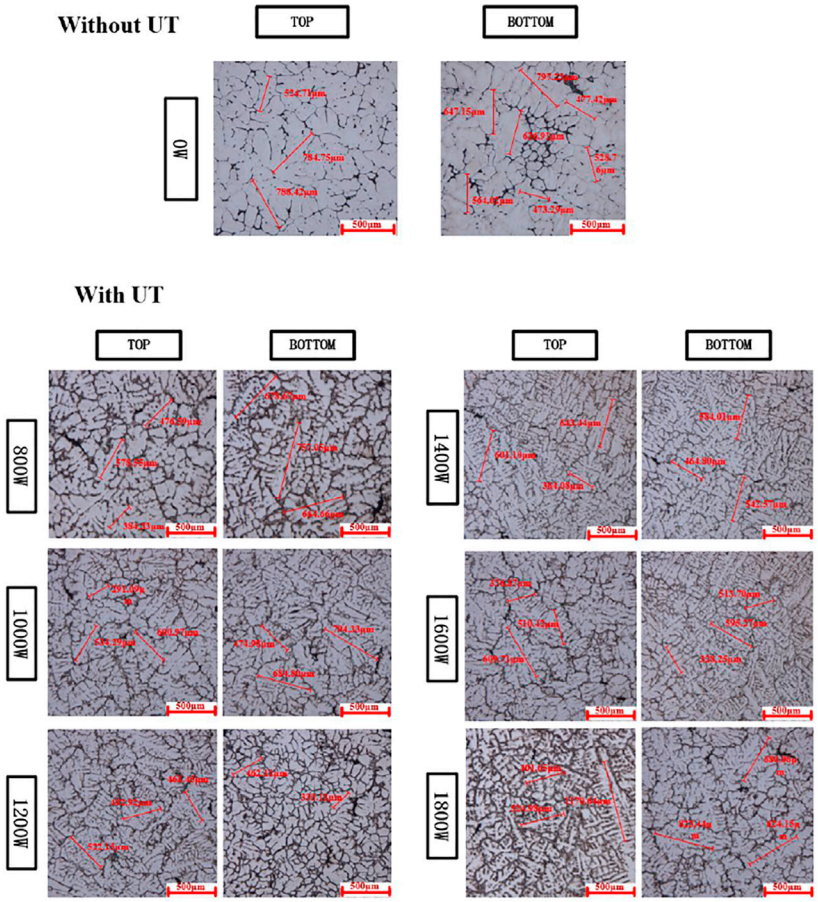

FIGURE 3 | Ultrasonic processing of optical micrographs of the top and bottom parts of 2195.

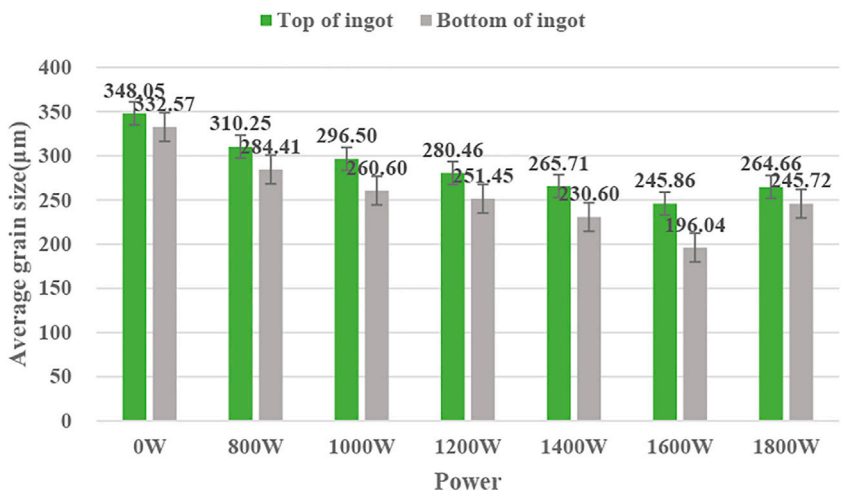

FIGURE 4 | Average grain measure of α-Al grains at agent positions of ingots treated with diverse ultrasonic powers.

the linear intercept method [ASTM E112-13(2021)]. ICP (inductive coupled plasma emission spectrometer) was utilized to analyze the composition of a particular position of the ingot. The area fraction of the coarse eutectic phase and the density of the precipitated particles were counted using image quantitative analysis software (Image-Pro Plus, IPP).

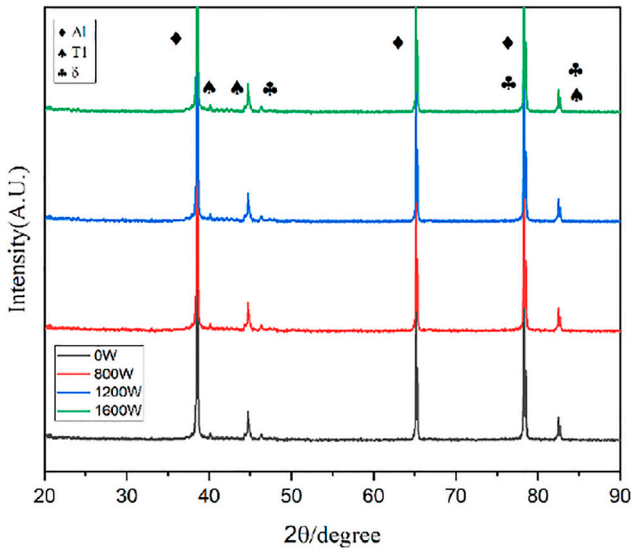

FIGURE 5 | X-ray diffraction spectrum of 2195 aluminum–lithium alloy ingot mainly containing Li phase.

RESULTS AND DISCUSSION

Microstructure of α-Al Phase

In **Figure 3**, the metallographic photos of the representative positions of the seven ingots were shown. They were the top of the ingot and the bottom of the ingot, respectively. Without UT in **Figure 3** shows that the ultrasonic vibrator does not work when the ultrasonic vibrator is inserted into the melt, and with UT in **Figure 3** shows the grain structure under different vibration power conditions. Obviously, under the ultrasonic treatment, the grain size at the two positions in the ingot was smaller than that of the ingot without UT.

Figure 4 measured the average size of α-Al grains in the two regions (top and bottom) of seven ingots under different ultrasonic powers. In the same test area of the ingot, the size of the α-Al grains first decreased and then increased, and the grain change trend showed a "V" shape with the increase of the ultrasonic power. When the ingot was cast under the condition of a total ultrasonic power of 800 W, the average size of the α-Al crystal grain at the bottom of the ingot was 330.25 μm. As the ultrasonic power increased to 1,600 W, the average size of the ingot was reduced to 215.45 μm. When the ultrasonic power was further increased to 1,800 W, the average size of α-Al grains increased to 245.72 μm. And the grain size of the ingot without UT was larger than that of the ingot with UT. The preliminary conclusion was drawn that when the ultrasonic power is maintained at 1,600 W, the α-Al grain refinement effect is the most significant. As shown in **Figure 3**, compared to the ingots with 1,600 W, it could be observed that the morphology of the α-Al particles in the ingots with 1,000 and 1,400 W was irregular even at the top position; a large number of dendrites were distributed. In fact, in the structure of the bottom of the ingot, the formation of equiaxed grains was mainly because the melt was poured into the mold, and the temperature of the mold was relatively low, resulting in a certain degree of supercooling.

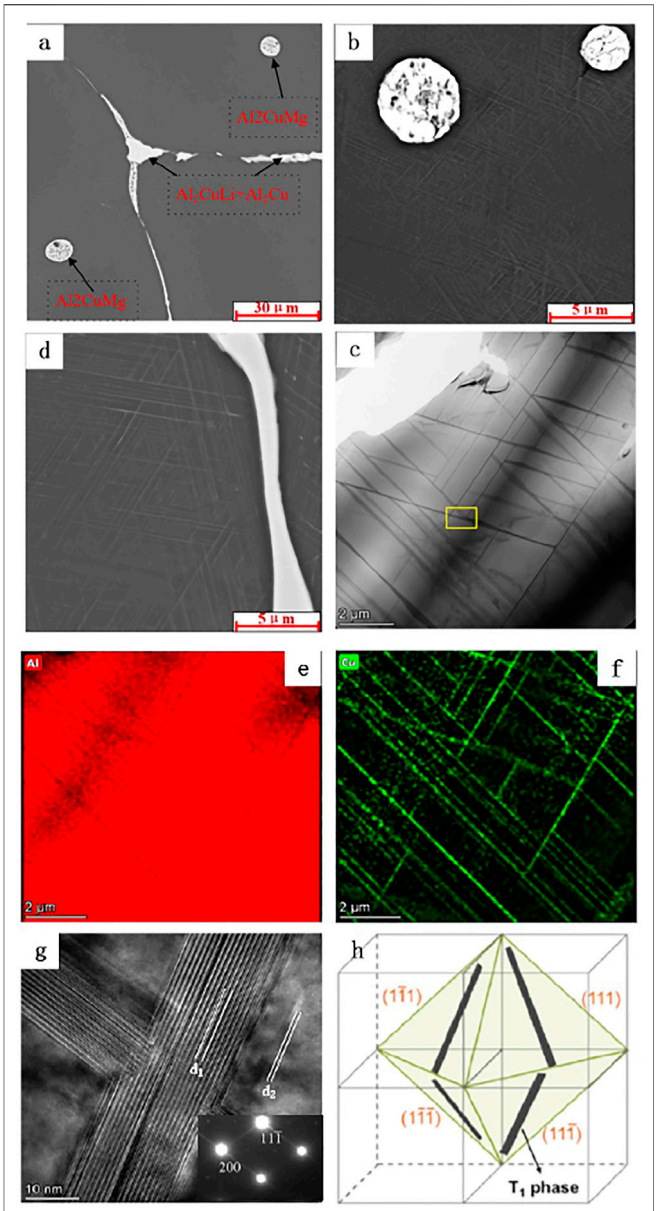

FIGURE 6 | X-ray diffraction spectrum of 2195 aluminum–lithium alloy ingot mainly containing Li phase. **(A–C)** Microstructure of ingot, **(D)** TEM bright-field image of needle-like phase, **(E,F)** EDS composition detection of needle-like phase, **(G)** high-resolution photo of T1 phase and Al matrix and diffraction spots, **(H)** four groups of T1 phase diagrams located on the (111) Al plane.

However, in the top, since the melt finally entered the melt during the casting process, the temperature of the mold raised, resulting in a decrease in the degree of supercooling and a much lower cooling rate. By measuring the changes of α-Al grain size under different ultrasonic powers, it is shown that the changes of ultrasonic power affect the microstructure of the ingot.

Because the ultrasonic vibrator material was titanium, trace quantity of titanium would enter the melt throughout the treatment procedure (Wang et al. (2014)). During the melting

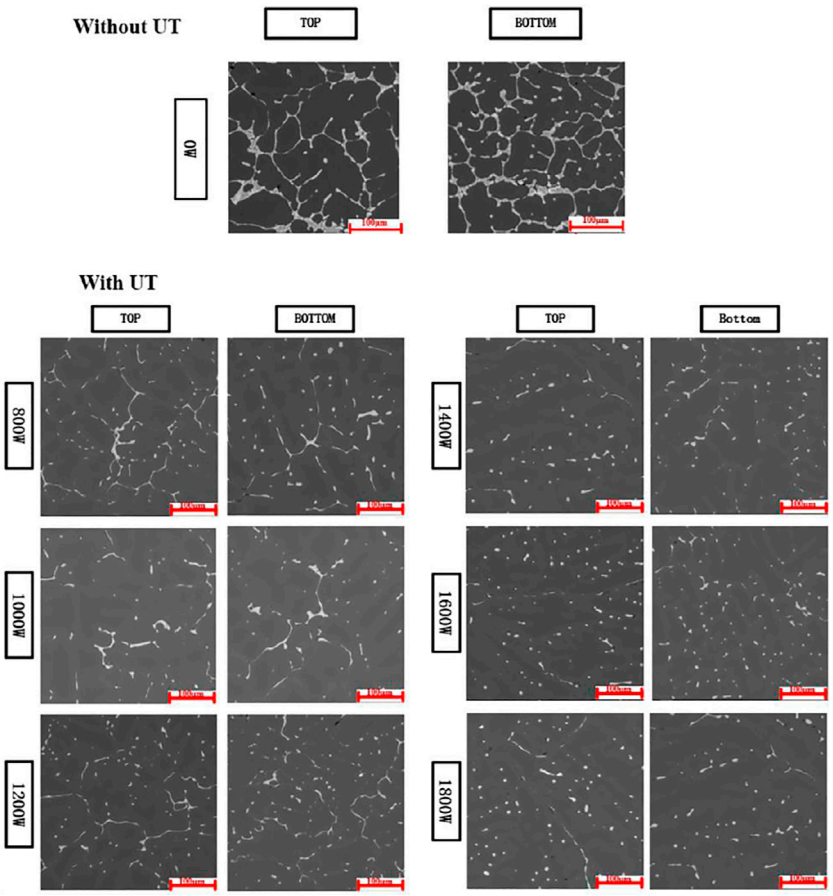

FIGURE 7 | SEM images of precipitated phases in representative positions of 2195 ingots under different ultrasonic power treatments.

process, the study discovered that ultrasound caused a huge number of cavitation bubbles to be formed. During the bursting phase, the cavitation bubble releases a lot of energy and creates forceful impact micro-jets. The continuous micro-jet may decrease pollution on the surface of molten particles, enhancing the particles' weaving resistance as a heterogeneous core portion. These nucleated particles might originate from *in situ* living particles or arise in the liquefied product. Numerous studies have demonstrated that $TiAl_3$, $ZrAl_3$, $NbAl_3$, and/or BTi_2 can be suitable nucleation sites. The grain fineness of α-Al grains improves when more potential nucleation particles are generated.

The test results reveal that ultrasonic power has a huge impact on the ingot's α-Al grain size. However, the refining effect does not always improve when the power of ultrasonic equipment grows. The refining impact is not as excellent as 1,600 W when the ultrasonic power is increased to 1,800 W. However, it is far superior to the 1,200 and 800 W cases. As a result, the power should be kept close to 1,600 W. The cavitation capacity may be efficiently increased by increasing the ultrasonic vibration power. The bursting of cavitation bubbles releases a tremendous amount of energy and expands the melt's range of action.

The cavitation and convection effects of ultrasonic vibrator power below 1,600 W were not as strong as those at ultrasonic vibrator power of 1,600 W. However, as the total power increased to 1,800 W, the size of the cavitation bubbles would increase to a very large extent during the expansion stage of ultrasound, causing the cavitation bubbles to not be in the compression stage immediately. This would produce a large number of useless cavitation bubbles, thereby increasing the attenuation of scattering and reducing the intensity of cavitation (Noltingk and Neppiras, 1950). On the other hand, the power of each ultrasonic vibrator was increased to 1,800 W. Li et al. (2016) related research on the influence of the multielement ultrasonic treatment on the melt. If the vibration power is too high, the reflected wave generated by the crucible wall will be too strong to cause irregular superposition or deviation of the acoustic oscillation wave, and change the effective vibration frequency in the melt. Nucleation has a great impact. At the same time, as shown in the related experiments by Sharma et al. (2009), this would weaken the liquid metal convection between the crystals, reduce the stirring effect on the solidification front, and is not conducive to the heat transfer and homogenization of the

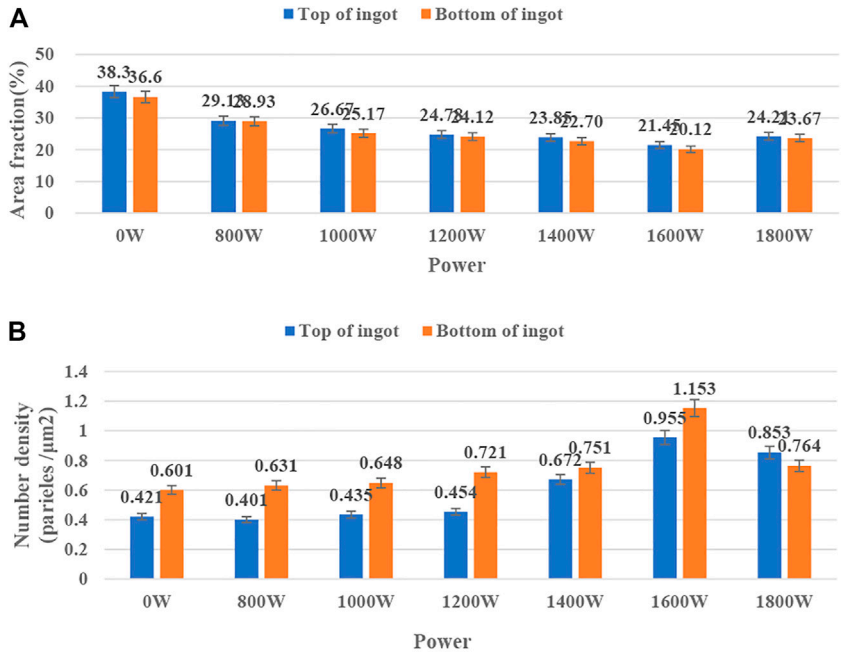

FIGURE 8 | (A) Area fraction of the precipitated phases with areas more than 20 μm^2 and **(B)** number density of the precipitated particles with areas less than 20 μm^2 at representative positions of 2195 ingots treated under different ultrasonic power.

TABLE 2 | Distribution of Cu and Mg content in grains of 2195 Al–Li alloy ingots at typical positions under different power conditions (wt%).

	0 W		800 W		1000 W		1200 W		1400 W		1600 W		1800 W	
	Cu	Mg	Cu	Mg	Cu	Mg	Cu	Mg	Cu	Mg	Cu	Mg	Cu	Mg
Top	1.24	0.086	1.37	0.086	1.36	0.099	1.48	0.124	1.56	0.134	1.76	0.193	1.66	0.154
Bottom	1.19	0.065	1.41	0.061	1.42	0.072	1.56	0.079	1.69	0.119	1.81	0.147	1.79	0.149
Mean	1.22	0.051	1.39	0.077	1.41	0.087	1.51	0.103	1.62	0.126	1.82	0.167	1.69	0.15

nucleated particles. Further research is ongoing to verify this speculation.

Distribution Characteristic of Eutectic Phase

The atomic number of the Li element was only 3. Due to the small atomic number, EDS energy spectrum analysis cannot measure its content and distribution in the alloy. Therefore, it was impossible to directly determine whether there was a eutectic phase of Li with the same content as T_1 in the alloy structure. Using XRD phase analysis, the X-ray diffraction spectra of the main Li-containing phase of the Φ60 mm-2195 Al–Li alloy ingot in **Figure 5** under different power states were obtained. It can be seen that the Li-containing alloy phases in the 2195 casting structure were mainly the T_1 (Al_2CuLi) phase and δ (AlLi) phase, and the phase did not change with the different ultrasonic power.

From the microstructure of the Φ60 mm-2195 Al–Li alloy ingot in **Figure 6A**, it can be observed that the coarse continuous eutectic structure was precipitated at the grain boundary, and also a large number of needle-like precipitates and needle-like phases were precipitated. The coarse eutectic phases grown on the grain boundaries were regularly precipitated according to a certain arrangement angle. The acicular phases precipitated on both sides of the same eutectic structure had different arrangement angles, and the eutectic structure and the needle-like precipitated phases directly existed in an approximately precipitate-free zone (PFZ) of about 1 μm. At the same time, similar needles precipitated in large quantities in the crystal grains according to a certain angle rule, which is shown in **Figure 6B**. The acicular phase with eutectic phase particles in the crystal grain had a larger distribution area in the crystal grain, and when there was no internal crystal grain or the distribution of fine eutectic phase is less. This kind of acicular phase was only distributed around the coarse eutectic structure near the grain boundary.

According to the XRD phase analysis and detection results (**Figure 5**), the main types of Li phases in the ingot structure were obtained, which were the T_1 (Al_2CuLi) phase and δ phase. The delta phase was an equilibrium phase with a cubic crystal structure and generally precipitates on the grain boundaries, so the needle-like phase was excluded as the delta phase.

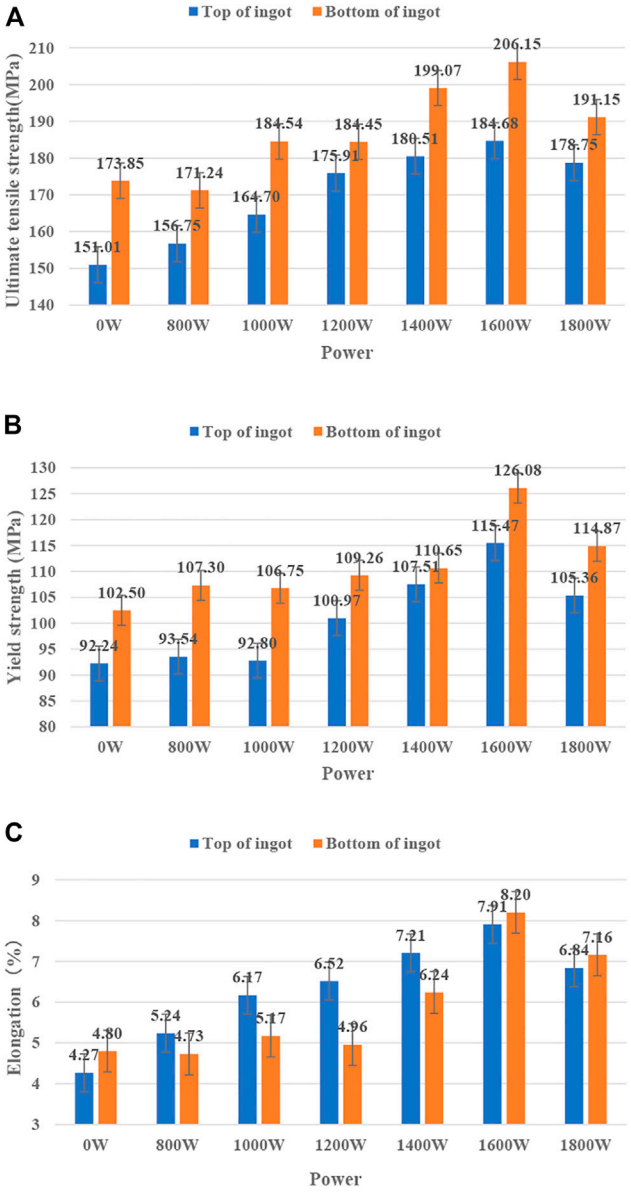

FIGURE 9 | (A) Ultimate tensile strength processed under different ultrasonic **(B)** yield strength and **(C)** elongation determined from different positions of the ingot.

According to the literature (Dorin et al., 2014), it can be observed that the T_1 (Al_2CuLi) phase was in the Al-based (111) Al crystal plane family. Observing the T_1 phase from a direction that was not perpendicular to the customary plane, the cross section of the T_1 phase shows a needle-like shape, as shown in **Figures 6A,B**.

Figure 7 shows the SEM results of different positions of the ingot under different ultrasonic powers. The precipitated particles from the small spherical eutectic structure shown in **Figure 7** are scattered in the α-Al crystal grains of the ingot. The eutectic phase at the top of the ingot is broader than the eutectic phase at the bottom, and the grain boundary has a flaky and continuous coarse eutectic structure. In the SEM picture of 1,200–1,600 W, it can be observed that the coarse eutectic structure in the solidified structure was reduced, and with the increase of the vibration power, the morphology of the eutectic structure and the continuous grain boundary have changed significantly. The eutectic network structure shrinks, the aggregation phenomenon is diminished, the eutectic structure's length and width are reduced, and the eutectic phase appears in the structure as a spherical form. However, when the vibration power was increased to 1,800 W, the amount of the eutectic structure accumulated on the grain boundary increased, and the continuity was enhanced.

The morphology of the eutectic structure on the grain boundary and the morphology of the eutectic precipitates inside the grains are different on the top and bottom of the ingot. The structure of the precipitated particle at the same position is exceptionally diverse, with ultrasonic treatment, particularly in 800 and 1,200 W ingots. The size of the eutectic phase at the ingot's upper and lower grain boundaries is greatly reduced at 1,600 W, and a high number of spherical eutectic phases develop in the α-Al grains. However, when the power is increased to 1,800 W, a coarse eutectic structure forms at the grain boundary.

The area fraction of the coarse eutectic structure on the grain boundary and the density of the point-like precipitation particles in the grain (the number of particles per unit area, the unit was μm^2) were measured, and the Image-Pro Plus software was used for evaluation. **Figure 7** shows the area fraction of the coarse eutectic phase with an area >20 μm^2 and the number density of spot-like precipitated phase particles with area <20 μm^2 in seven ingots.

As shown in **Figure 8A**, as the ultrasonic power increases, the number of coarse eutectic phases decreases, and the minimum number appears at the power condition of 1,600 W. The value is 3.45%. The area ratio of the coarse eutectic phase of the ingot at 1,600 W is reduced by 30.45% (from 28.93% to 20.12%) from the top to the bottom of the ingot, and the value is higher than 1,600 W in other power states of the ingot. Regarding the density of the dot-like precipitated particles, the ingots cast at 1,600 W increased by 147.5% (from 0.631 to 1.153) compared to those at 800 W. However, with the increase of ultrasonic power, the value of the top and the bottom part of the ingot cast at 1,800 W is higher than that of the ingot at 1,600 W. Therefore, by setting the ultrasonic power reasonably during the solidification process, both the primary α-Al grains and the precipitated phases are refined.

As seen in **Figure 8B**, the density of precipitated particles within the ultrasonicated ingots changes marginally; the least value at the best is 1.153%, and it steadily increases to 0.751% at the bottom. For the comparing value within the ingot without UT, the least of the bottom position is 0.401%.

The Cu and Mg contents in the grains of the typical region of Φ60–650 mm 2195 Al–Li alloy ultrasonic ingots under different power conditions were tested. The test results are shown in **Table 2**. According to the test results, the average Cu content distribution in the crystal grains can be found that with the increase of the vibration power the average Cu content in the crystal grains also increased. Similarly, the Mg element also had a similar distribution law with the increase of solute elements in the crystal grains. This made it easier for the fine eutectic particles in the grains to precipitate in grains. At the same time, the test

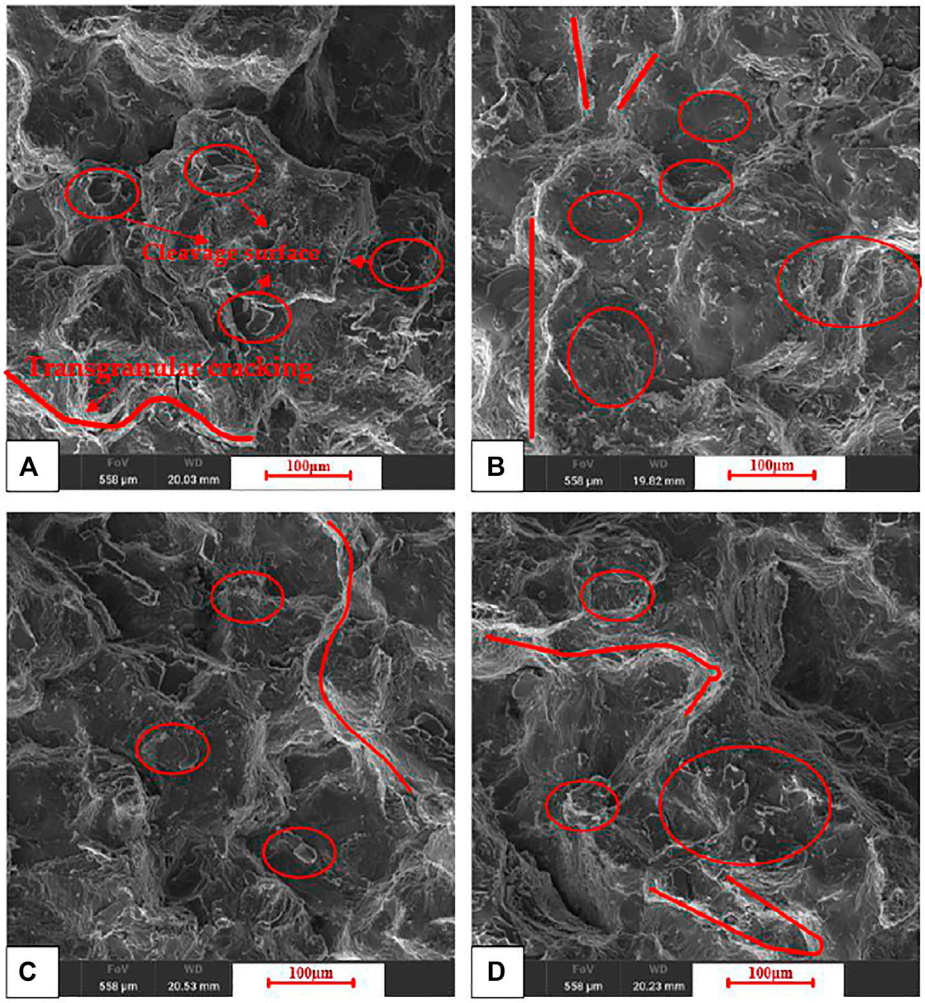

FIGURE 10 | SEM images of the tensile fracture surfaces in ingots cast under a total ultrasonic power of **(A)** 800 W, **(B)** 1,200 W, **(C)** 1,600 W, and **(D)** 1,800 W.

results indicated that the solute elements were significantly increased in the aluminum matrix, which indicated that there were more solute atoms in the matrix. According to the relevant research of Zhang et al. (2016), it was proven that as the solute atoms increase, the lattice distortion energy in the system will follow. There was pin dislocation movement, thereby increasing the strength of the material.

Second, where the area distribution of the eutectic structure is relatively large, the intragranular copper content and the number density of the granular eutectic phase are relatively small, resulting in the reduction of intragranular Cu content and the granular eutectic phase. In addition, the microscopic Cu content of the ingot should be the Cu content in the eutectic structure, the intercrystalline Cu content, and the Cu content in the grain eutectic phase, the sum of the three. This study can only show that in areas where the coarse eutectic structure is widely distributed, the intragranular Cu content and the number of eutectic particles are low, which will damage the subsequent deformation treatment process. Therefore, the formation of the coarse eutectic structure should be reduced during the casting process. The amount of eutectic structure was of great significance to the preparation of qualified materials.

Mechanical Properties

The test sample is taken according to the position in **Figure 2** to test the mechanical properties of the ingot. The test results in **Figures 9A–C** show the tensile strength (UTS), yield strength (YS), and elongation of the ingot, respectively.

Tensile strength, yield strength, and elongation are three indicators used to compare ingots with different ultrasonic powers in the axial direction. At the bottom of the ingot, the ingot is slightly higher than the top area of the ingot, but the overall value difference is small. The tensile strength of the bottom area of the ingot is generally higher than that of the middle area of the ingot, except for the tensile strength near 1,800 W. Under other vibration power conditions, the tensile strength increases as the power increases. The maximum value appears near the vibration power of 1,600 W, which is 206.15 MPa. The main reason for the decrease of the mechanical properties of the ingot with a vibration power of 1,800 W is the appearance of a coarse eutectic structure in

the solidification structure. The yield strength gradually increased from 93.54 MPa at 800 W to 115.47 MPa at 1,600 W, and the maximum value appeared at the bottom area of the 1,600 W ingot at 206.15 MPa. The elongation change trend was similar to the tensile strength change trend. Both have the lowest value near 800 W, which was 4.73%. With the increase of vibration power, the elongation of the ingot also increased, and the maximum value was 8.20% near 1,600 W.

To further analyze the relationship between the eutectic structure and mechanical properties, the fracture behavior of the ingot was studied. **Figure 10** shows the fracture morphology of the tensile specimen in the middle region of the ingot under different vibration power states. From **Figure 10**, it can be seen that there were rough tearing edges on all the fractures, and the surface of the fractures was covered with a large number of white granular eutectic fragments. In addition to tearing edges on the fracture surface of the 800 W sample, there were also traces of fracture along the grain boundary. The fracture surface contains deep dimples to varying degrees. However, the fracture surfaces of 1,200 and 1,600 W were covered with latent dimples of similar size, and the rough fracture surface of the fracture was greatly reduced. Most of them were smoother fracture surfaces along the grain boundary, and the dimples were uniform. The eutectic structure had a higher elastic modulus than the Al matrix. When the structure was deformed by an external force, the eutectic phase tended to produce elastic deformation (Lys et al., 2020). Due to the different elastic modulus, microcracks will appear in the particles first around. When the size and quantity of the eutectic structure in the matrix were large, it will cause rapid growth of cracks. As a result, the sample quickly fractures and fails during the tensile deformation process, resulting in a decrease in mechanical properties.

The Hall–Petch formula is adopted as presented in **Eq. 1**:

$$\sigma_s = \sigma_0 + Kd^{-\frac{1}{2}}, \quad (1)$$

where σ_s is the surrender quality, σ_0 is the fabric consistent, K is the Hall–Petch incline, and d is the normal grain estimate (Hansen. 2004). The strength of the material is inversely proportional to the grain size (Nadella et al., 2008). Therefore, He et al. (2018)stated that the finer the grains of the ingot, the better the mechanical properties. Nevertheless, the changes in the mechanical properties of the 2195 ingot cannot be mainly attributed to the refinement of the basic α-Al grains. According to Thacker, (1973), when the material undergoes tensile deformation, the coarsening of the eutectic structure is the initial location for cracks. As shown in **Figure 9**, there were a large number of coarse precipitated phase networks in a and b, Therefore, reducing the coarsening precipitates played an important role in improving the mechanical properties. Al-Helal et al. (2018) have been demonstrated that an increase in quality comes at the expense of ductility under conventional conditions, but fine α-Al grains that were consistently disseminated and accelerated can increase both quality and ductility at the same time. Round particles can reduce the stress concentration generated during deformation, subsequently increasing the ductility of the aluminum combination. Therefore, under UT, as the coarsening precipitates decrease and the fine precipitates increase, the elongation of the sample was increased accordingly.

CONCLUSION

This study compared the effects of different power ultrasonic systems on the morphology, α-Al grain size, eutectic phase, and mechanical properties of 2195 Al–Li ingots. The main conclusions can be summarized as follows:

(1) The shape of α-Al crystal grains and eutectic precipitates is greatly influenced by ultrasonic vibration power. The ultrasonic system with 1,600 W power has the most noticeable influence on the refining of α-Al grains and precipitates when compared to other powers. The area of the coarse eutectic structure is decreased by 47.46%, and the density of precipitated particles in the crystal grains is enhanced by 91.84% when the power is increased to 1,600 W. The α-Al grain size in the bottom portion of the ingot is much smaller than that in the top region, as is the coarse eutectic phase size and precipitation phase density.
(2) As the vibration power increases from 800 W to 1,600 W, the area fraction gradually decreases. The eutectic structure in the crystal grains is more obvious in the form of small-size precipitation than the continuous coarser morphology distributed along the grain boundary. When the matrix is deformed by an external force, the dispersed and precipitated eutectic phases will play a role in pin dislocations, hinder the deformation of the entire system, improve the tensile properties of the material, and thereby increase the tensile strength and yield strength of the material. In summary, the ultrasonic vibration power in the molten pool should be set near 1,600 W. In this power range, the cavitation and acoustic flow effects generated by the ultrasonic waves applied to the molten pool will affect the temperature field and flow field in the entire molten pool so that the uniformity of the solidification structure of the ingot can be controlled most effectively.

DATA AVAILABILITY STATEMENT

The original contributions presented in the study are included in the article/Supplementary Materials, further inquiries can be directed to the corresponding author.

ETHICS STATEMENT

Written informed consent was obtained from the individual(s) for the publication of any potentially identifiable images or data included in this article.

AUTHOR CONTRIBUTIONS

YH was responsible for writing the full paper, and carefully manipulated the experiments in the paper to verify the authenticity of the experimental data. RJ was responsible for revising the paper and explaining the mechanism of the experimental phenomena. XL was responsible for the overall work, the development of the experimental protocol, and the structure of the thesis.

FUNDING

The study was funded by the National Natural Science Foundation of China (Grant No. 51805549).

ACKNOWLEDGMENTS

Technicians at Light Alloy Research Institute of Central South University are thanked for providing experimental assistance.

REFERENCES

Abramov, O. V. (1999). *High-Intensity Ultrasonics: Theory and Industrial Applications*. 1st ed. Boca Raton: CRC, 200–217.

Al-Helal, K., Chang, I., Patel, J. B., and Fan, Z. (2018). Thermomechanical Treatment of High-Shear Melt-Conditioned Twin-Roll Cast Strip of Recycled AA5754 alloy. *JOM*, 1–7. doi:10.1007/s11837-018-3190-8

Blankenship, C. P., and Kaisand, L. R. (1996). Elevated Temperature Fatigue Crack Propagation Behavior of an Al-Li-Cu-Mg-Ag-Zr alloy. *Scripta Materialia* 34 (9), 1455–1460. doi:10.1016/1359-6462(95)00680-x

Dorin, T., Deschamps, A., De Geuser, F., Lefebvre, W., and Sigli, C. (2014). Quantitative Description of the T1formation Kinetics in an Al-Cu-Li alloy Using Differential Scanning Calorimetry, Small-Angle X-ray Scattering and Transmission Electron Microscopy. *Phil. Mag.* 94 (10), 1012–1030. doi:10.1080/14786435.2013.878047

El-Aziz, A. M., El-Hady, M. A., and khlifa, W. (2016). in *Effect of High Intensity Ultrasonic Treatment on the Microstructure, Corrosion and Mechanical Behaviour of AC7A Aluminum Alloy*. Editor E. Williams (New York: Springer), 721–724. doi:10.1002/9781119274780.ch121

Eskin, G. I., and Eskin, D. G. (2014). *Ultrasonic Treatment of Light Alloy Melts*. 2nd ed. Boca Raton: CRC.

Eswara Prasad., N., Amol, A. G., and Yamhill, R. J. H. (2014). *Aluminum-lithium Alloys*, 45. Elsevier, 78–85.

Hansen, N. (2004). Hall-Petch Relation and Boundary Strengthening. *Scripta Materialia* 51, 801–806. doi:10.1016/j.scriptamat.2004.06.002

He, H., Yi, Y., Huang, S., and Zhang, Y. (2018). Effects of Deformation Temperature on Second-phase Particles and Mechanical Properties of 2219 Al-Cu alloy. *Mater. Sci. Eng. A* 712, 414–423. doi:10.1016/j.msea.2017.11.124

Huang, H. J., Yi-Fan, X., Shu, D., Han, Y-F., Wang, J., and Sun, B-d. (2014). Effect of Ultrasonic Melt Treatment on Structure Refinement of Solidified High Purity Aluminum[J]. *Trans. Nonferrous Met. Soc. China* 24 (7), 24142419. doi:10.1016/s1003-6326(14)63365-3

Jata, K. V., Hopkins, A. K., and Rioja, R. J. (1996). The Anisotropy and Texture of Al-Li Alloys. *Msf* 217-222, 647–652. doi:10.4028/www.scientific.net/msf.217-222.647

Kang, J.-w., Sun, X.-f., Deng, K.-k., Xu, F.-j., Zhang, X., and Bai, Y. (2017). High Strength Mg-9Al Serial alloy Processed by Slow Extrusion. *Mater. Sci. Eng. A* 697, 211–216. doi:10.1016/j.msea.2017.05.017

Li, A. Q., Jiang, L. H., Zhang, R. P., and Li, , X. Q. (2021). Effect of Cooling Speed and Ultrasonic Vibration on Solidification Structure and Mechanical Properties of 7085 Aluminum Alloy[J]. *J. Mater. Eng.* 49 (8), 63–71. doi:10.11868/j.issn.1001-4381.2020.001142

Li, R. Q., Liu, Z. L., Dong, F., Li, X. Q., and Chen, P. H. (2016). Grain Refinement of a Large-Scale Al alloy Casting by Introducing the Multiple Ultrasonic Generators during Solidification. *Metall. Mater. Trans. A.* 47, 3790–3796. doi:10.1007/s11661-012-1155-z

Li, X., Jiang, R., Chen, P., Li, R., and Zhang, X. (2014). Effect and Kinetic Mechanism of Ultrasonic Vibration on Solidification of 7050 Aluminum Alloy[J]. *AIP Advances* 4 (7), 77125. doi:10.1063/1.4891035

Li, X. Q., Li, R. Q., Dong, F., Chen, P., and Jiang, R. (2015). *Simulation and Experimental Study of Cavitation Region Caused by Longitudinal and Transverse Vibration of Casting Ultrasonic radiator[C]//Materials Science and Engineering Conference Series.* in *Materials Science and Engineering Conference Series*, 0520.

Lys, A., Bnd, A., Zyha, D., Yxq, B., Zpx, B., Bjw, A., et al. (2020). Effects of Annealing Treatment on Microstructure and Tensile Behavior of the Mg-Zn-Y-Nd alloy. *J. Magnesium Alloys* 8 (3), 601–613. doi:10.1016/j.jma.2019.07.011

Nadella, R., Eskin, D. G., Du, Q., and Katgerman, L. (2008). Macrosegregation in Direct-Chill Casting of Aluminium Alloys. *Prog. Mater. Sci.* 53, 421–480. doi:10.1016/j.pmatsci.2007.10.001

Noltingk, B. E., and Neppiras, E. A. (1950). Cavitation Produced by Ultrasonics[J]. *Proc. Phys. Soc. Lond.* B63, 647. doi:10.1088/0370-1301/63/9/305

Rioja, R. J., and Liu, J. (2012). The Evolution of Al-Li Base Products for Aerospace and Space Applications. *Metall. Mat Trans. A.* 43 (9), 3325–3337. doi:10.1007/s11661-012-1155-z

Sharma, V. M. J., Kumar, K. S., Rao, B. N., and Pathak, S. D. (2009). Effect of Microstructure and Strength on the Fracture Behavior of AA2219 alloy. *Mater. Sci. Eng. A* 502, 45–53. doi:10.1016/j.msea.2008.11.024

Thacker, J. (1973). An Approach to the Mechanism of Killing of Cells in Suspension by Ultrasound. *Biochim. Biophys. Acta (Bba) - Gen. Subjects* 3042, 240–248. John. doi:10.1016/0304-4165(73)90241-9

Wang, G., Dargusch, M. S., Qian, M., Eskin, D. G., StJohn, D. H., and Growth, J. Cryst. (2014). The Role of Ultrasonically Induced Acoustic Streaming in Developing Fine Equiaxed Grains during the Solidification of an Al-2 Pct Cu Alloy. *J. Cryst. Growth* 408, 119–124. doi:10.1016/j.jcrysgro.2014.09.018

Zhang, L., Eskin, D. G., and Katgerman, L. (2011). Influence of Ultrasonic Melt Treatment on the Formation of Primary Intermetallics and Related Grain Refinement in Aluminum Alloys. *J. Mater. Sci.* 46, 5252–5259. doi:10.1007/s10853-011-5463-2

Zhang, L., Li, R., Jiang, R., Zhang, L., and Li, X. (2019). A Comparative Study on the Effect of Four-Source Ultrasonic Power on the Microstructure and Mechanical Properties of Large-Scale 2219 Aluminum Ingots. *JOM*. doi:10.1007/s11837-019-03459-y

Zhang, L. H., Li, H. X., Li, C., Li, Z., Li, R., and Dong, F. (2016). Interfacial Bonding Mechanism of SiCp/7085 Composites Under Ultrasonic External Field[J]. *J. Cent. South Univ.* 47 (9), 8. doi:10.11817/j.issn.1672-7207.2016.09.009

Conflict of Interest: The authors declare that the research was conducted in the absence of any commercial or financial relationships that could be construed as a potential conflict of interest.

Publisher's Note: All claims expressed in this article are solely those of the authors and do not necessarily represent those of their affiliated organizations, or those of the publisher, the editors, and the reviewers. Any product that may be evaluated in this article, or claim that may be made by its manufacturer, is not guaranteed or endorsed by the publisher.